Analyst

Accepted Manuscript

This article can be cited before page numbers have been issued, to do this please use: Y. Zhao, Y. Wang, S. Liu, C. Wang, J. Liang, S. Li, X. Qu, R. Zhang, J. Yu and J. Huang, *Analyst*, 2019, DOI: 10.1039/C9AN00953A.

DOI: 10.1039/C9AN00953A

Triple-helix Molecular Switch-actuated Exponential Rolling Circular Amplification for Ultrasensitive Fluorescence Detection of miRNA

Yihan Zhao[a], Yu Wang[a], Su Liu[b], Chonglin Wang[a], Jiaxu Liang[a], Shasha Li[a], Xiaonan Qu[b] , Rufeng Zhang[b], Jinghua Yu[c] , Jiadong Huang [a c*]

a School of Biological Sciences and Technology, University of Jinan, Jinan 250022, P.R. China.

b School of Water Conservancy and Environment, University of Jinan, Jinan 250022, P.R. China.

c Key Laboratory of Chemical Sensing & Analysis in Universities of Shandong, School of Chemistry and Chemical Engineering, University of Jinan, Jinan 250022, P.R. China

*Corresponding Author. E-mail: chm_huangjd@ujn.edu.cn; Tel.:+86-531-89736122; Fax:+86-531-82769122.

View Article Online
DOI: 10.1039/C9AN00953A

Abstract

We have established a rapid and high-efficiency fluorescent biosensing platform based on target-activated the triple-helix molecular switch (THMS) conformation change-induced exponential rolling circular amplification (RCA) strategy for ultrasensitive detection of miR-21. In this strategy, there are several aspects that make sense. First of all, the functionalized THMS, containing a typical triplex structure (T-A·T), a specific recognition sequence for nicking endonuclease, a complementary sequence for miR-21 and an RCA product-annealing sequence, was concurrently used to perform signal transduction with one fluorophore and one quencher. Compared to the traditional double-helix molecular switches or molecular beacon, one of the biggest differences is that the property of THMSs is independent of any special binding sequence it contains. As far as we know, this is the first time that the ingenious designed THMS not only contains the primer for exponential RCA but also functions as the tracer for the fluorescence assay. In the presence of miR-21, targets can induce the conformation change of THMS with the release of the trapped DNA segment (P) which can activate first-run RCA process. Meanwhile, the RCA reaction is also initiated by the formation of similar primer (SP) as the trapped DNA through a continuous "extension-nicking" reaction. Secondly, the resultant first-generation RCA product consists of numerous tandem repeated region that can attach countless of THMS, resulting in the release of the trapped DNA segment (P) for initiating second-run RCA reaction. Significantly, a large amount of THMS was continuously consumed to generate a remarkably strong fluorescent signal readout. Additionally, this biosensor was demonstrated to exhibit improved sensitivity owing to the high efficiency and rapid amplification kinetics of exponential RCA and high selectivity toward miR-21 with a limit of detection as low as 1.1 aM. Hence, the target-mediated the switch change of THMS-initiated exponential RCA strategy presents an optimal detection performance towards analytes for potential application in related fundamental research and clinical diagnosis.

Keywords: Triple-helix molecular switch; Rolling circular amplification; miR-21; Fluorescence detection

View Article Online
DOI: 10.1039/C9AN00953A

1. Introduction

MicroRNAs (miRNAs) are widely found in eukaryotes and are a group of short-sequence RNAs (18-25 bases) that do not encode proteins.[1-4] They play an important role in cell proliferation, migration, differentiation, and apoptosis. The abnormal expression of miRNAs is closely related to cancer, cardiovascular diseases and autoimmune diseases.[5-7] Conventional techniques for miRNAs detection mainly include quantitative real-time polymerase chain reaction (qRT-PCR),[8] microarrays,[9] northern blotting,[10] electrochemical[11] and photoelectrochemical-based assays[12]. Although these methods afford high sensitivity, they suffer from the shortcomings of fussy and time-consuming operations, sophisticated equipments, and professional technical personnel. Therefore, the development of sensitive and specific sensing strategies for detecting miRNAs is of great significance to the understanding of biological function and early diagnosis of disease.

Up to now, isothermal amplification techniques, such as hybridization chain reaction (HCR),[13-15] strand displacement amplification (SDA),[16-18] rolling circle amplification (RCA),[19-23] and exonuclease or endonuclease-based amplification, have been widely exploited for the construction of sensing platforms with improved sensitivities in modern biology and biomedicine. Among them, RCA has been regarded as the most frequently used amplification methods, which can achieve an extremely long single-stranded DNA (~15000 bases) with thousands of tandem repeats that are capable for inducing the assembly of signal probes (SP) or the configuration transform of SP. There is no doubt that the acquirement of primer is crucial for the RCA development process. Often target-mediated generation of RCA primer is generally employed in sensing applications. For example, Liu and co-authors developed a highly sensitive electrochemical method for detecting concanavalin A based on target-triggered proximity ligation accompanying with formation of a three-way DNA junction for RCA reaction.[24] Tang and co-authors reported a facile colorimetric assay system for protein detection using target-aptamer binding-initiated RCA reaction.[25] Xie's team proposed the RNA detection by coupling toehold exchange with RCA through nucleolytic conversion of a structure-switched

hairpin probe.[26] However, in these assays, one target molecule can only induce the formation of one RCA primer, which would affect the amplification efficiency adversely. In this regards, our starting point is to exploit novel exponential RCA strategy for achieving the formation of more RCA primers through the structure transformation of especial molecular switch, which aiming to improve amplification efficiency of RCA.

Recently, a triple-helix molecular switch (THMS) constructed by Watson-Crick and Hoogsteen base pairings has attracted extensive attention of researchers in bioassay.[27-30] THMS is commonly comprised of two DNA strands: an anti-target aptamer sequence with two short-armed complementary fragments, and a DNA sequence trapped between the arm fragments. It has been reported that THMSs have similar stability to the duplex DNA and high binding affinity with targets. THMS system has been industriously exploited for diverse applications including nucleic acid detection, protein detection, metal ion detection, and cell imaging. For example, Xuong et al. developed a simple and reusable electrochemical assay method for nucleic acid detection by the combination of THMS with dual signaling radiometric strategy.[31] Yang et al. presented a novel fluorescence resonance energy transfer (FRET) immunoassay strategy for sensitive detection of mucin 1 based on protein-mediated DNA assembly constructed by proximity binding-induced RCA.[32] Yang's group demonstrated a gold nanoparticle integrated programmable THMS to realize the simultaneously imaging of multiple mRNAs in living cells.[33] Lately, Ricci's group reported a new class of triple helix-based nanomachine that can reversibly load and release a molecular cargo on binding of a specific target antibody.[34] Although DNA triple helix has been explored as molecular device or molecular switch beacon,[29, 35-37] it is still essential to tap deeper potential to expand the applications in biosensing and bioimaging.

Herein, we have developed a rapid and high-efficiency fluorescent biosensing strategy based on target-activated the formation of RCA primer through the conformation change of THMS for ultrasensitive detection of miRNA. MiR-21 is selected as a model analyte. miR-21 is considered as a potential biomarker, its

overexpression is closely related to lung cancer and breast cancer. Our proposed strategy relies on target-induced conformation switch of THMS that is changed from "switch off" to "switch on", thus the trapped DNA is released and initiated high efficient exponential RCA reaction. It is noteworthy that since the TAT triplets are not sensitive to pH and are relatively stable at neutral pH,[28,30] the TAT triplets are introduced to ensure the high stability of the triple-helix structure in the reaction system. In our assay, a fluorophore/quencher pair-labeled THMS that comprises of a typical triplex structure (T-A · T), a specific recognition sequence for nicking endonuclease, a complementary sequence for miR-21, and a RCA product-annealing sequence is ingeniously designed, which functions as both the primer for RCA reaction and the tracer for fluorescence signal output. Compared to the existing RCA-based methods,[32] excepted for target-mediated formation of RCA primer, a cyclic "extension-cleavage" reaction is activated by target with the aid of phi29 and *Nt. BbvcI*, generating a large number of single-stranded DNA that acts as secondary primer for initiating RCA. Not only that, the resultant first-run RCA products consist of numerous tandem repeated sequence that can hybridize with the loop of THMS, resulting in the release of numerous primers for initiating second-run RCA process. On the basis of the high-efficient exponential RCA strategy, our proposed strategy are capable for detecting miRNA with high sensitivity. Thus, the THMS-actuated exponential RCA strategy might create a simple and robust fluorescence sensing platform for miRNA detection and related fundamental research and clinical diagnosis.

2. Experimental section

2.1 Materials and Reagents

All oligonucleotides (Table 1) were HPLC-purified and obtained from Shanghai Sangon Biological Engineering Technology &Services Co. Ltd. (Shanghai, China). phi 29 DNA Polymerase, *Nt.BbvcI*, T4 DNA ligase, 10×T4 DNA ligase reaction buffer (50 mM Tris-HCl, 10 mM $MgCl_2$, 10 mM DTT, 1mM ATP, pH 7.5), *E. coli* exonuclease I (Exo I), *E. coli* exonuclease III (Exo III), deoxynucleotide (dNTP)

solution mix, were obtained from New England Biolabs (Ipswich, MA, USA). $MgCl_2$, KCl, Tris-HCl were of analytical grade and purchased from Aladdin (Shanghai, China, www.aladdin-e.com). All solutions were prepared with ultrapure water (Millipore, Milford, MA).

2.2 Apparatus

Fluorescence measurements were carried out by using a Cary Eclipse Fluorescence Spectrophotometer (Hitachi, Japan) with excitation at 486 nm. Both the excitation and emission slit widths were set at 5 nm. Gel electrophoresis was conducted using DYCZ-24DN electrophoresis cell (LIUYI, Beijing, China) and Bio-Rad Gel imaging system (Bio-Rad, USA).

Table 1 DNA oligonucleotides sequence used in this work

Oligonucleotide name	sequence description (5' to 3')
molecular switch	FAM-TTTTTTTTTTTTTTGCTGAGGTCAACATCAGT CTGATAAGCTAGTCTGCCTTTTTTTTTTTTTT-BHQ1
trapped DNA (P)	AAAAAAAAAAAAAAA
linear padlock probe	P-GAGCATGCCCTGGACGGACGTCTGCCTTTTTTTT TTTTTTCTGTTCGCC
ligation probe	GGCATGCTC GGCGAACAG
miR-21	UAGCUUAUCAGACUGAUGUUGA
miR-144	GCUGGGAUAUCAUCAUAUACUG
let-7a	UGAGGUAGUAGGUUGUAUAGUU
miR-141	UAACACUGUCUGGUA AAGAUGG
miR-155	UUAAUGCUAAUCGUGAUAGGGGA

2.3 Preparation of the triple-helix molecular switch (THMS)

For the preparation of the triple-helix molecular switch, the THMS consists of a molecular beacon probe, modified with the fluorophore/quencher (FAM/BHQ1), and a trapped DNA (P). The 10 μM molecular beacon probe and the 10 μM trapped DNA (P) was added in 20 μL of buffer (50 mM Tris-HCl, 10 mM $MgCl_2$, 150mM KCl, pH 7.4) at 30 °C for 3h to form the THMS.

2.4 Preparation of the circular probe(CP) that is resistant to enzymatic degradation

For the preparation of the circular probe. The 30 μL CP reaction system consists of 3 μL 100 nM padlock probe and 3 μL 100 nM ligation probe, and 3 μL 10×T4 DNA ligase reaction buffer (50 mM Tris-HCl, 10 mM $MgCl_2$, 10 mM DTT, 1 mM ATP, pH7.5) was incubated at 95 °C for 5 min, then slowly cooled down to room temperature. Then 3 μL of 20 U μL^{-1} T4 DNA ligase was added and incubated at 20 °C for 4 h, Subsequently, the temperature was increased from 20 °C to 65 °C for 10 min to inactivate the T4 DNA ligase. After that, 1 μL of 20 U μL^{-1} Exo I and 1 μL of 100 U μL^{-1} Exo III were added CP reaction system at 37 °C for 2 h to digest the free and hybridized probe. Afterwards, the temperature was increased from 37 °C to 80 °C for 20 min to inactivate the Exo I and Exo III, then the resultant products were stored at 4 °C.

2.5 MiR-21 detection

All reactions were prepared in buffer (50 mM Tris-HCl, 10 mM $MgCl_2$, 150mM KCl, pH 7.4) for the detection of miR-21. Firstly, 4 μL 10 μM THMS, 1 μL 100 nM CP, 2 μL various concentrations of miR-21, 2 U mL^{-1} phi 29, 2 μL 1 mM dNTPs (10 mM dATP, dGTP, dCTP, dTTP each) and 1 U mL^{-1} *Nt.BbvCI*, which were performed in a volume of 20 μL at 30 °C for 4 h. After this time, the resultant product was mixed with 80 μL of ultrapure water and scanned using Agilent Cary Eclipse Spectrofluorometer. Unless noted otherwise, all experiments for miR-21 measurements were repeated three times in this study.

2.6 Preparation of the samples from cellular extracts

A breast cancer cell (MCF-7) and a pancreatic cancer cell line (AsPc-1) were obtained from the cell bank of the type culture collection of the Chinese Academy of Sciences (Shanghai, China). MCF-7 and AsPc-1 were cultured at 37 °C in a humidified 5% CO_2 incubator in RPMI medium 1640 supplemented with 10% fetal bovine serum (FBS) and 100 U/mL penicillin streptomycin. The cells were grown with fresh medium at 100 mm cell culture bottles. Total RNA from these cells was extracted using Trizol reagent according to the manufacturer's recommended protocol.

Cell samples was added to the lysis solution (1 mL Trizol), leave it at room temperature for 5 min to fully lyse. Subsequently, the mixture was centrifuged for 5 min at revolving speed of 12000 rpm, the supernatant was taken, and 200 μL of chloroform was added, shook mixture and left at room temperature for 15 min. The supernatant was taken out from the mixture, and 0.5 mL of isopropyl alcohol was added to the supernatant, and uniformly mixed at room temperature for 10 minutes. Afterward, centrifuge for 10 min at 12000 rpm at -4℃. And then remove the supernatant and wash by 75 % ethanol with DEPC water and centrifuge for 5 min at 8000 rpm at -4℃. Volatile ethanol to obtain purified total RNA

2.7 RT-PCR detection

The 10 μL PCR reaction included 0.67 μL RT product, 1×TaqMan, 0.2 μM TaqMan probe, 1.5 μM forward primer and 0.7 μM reverse primer. The reactions were incubated in a 384-well plateat 95℃ for 10 min, then for 40 cycles, 95 ° C for 15 seconds, and 60 ° C for 1 min.

3. Results and discussion

3.1 Principle of the proposed strategy

View Article Online
DOI: 10.1039/C9AN00953A

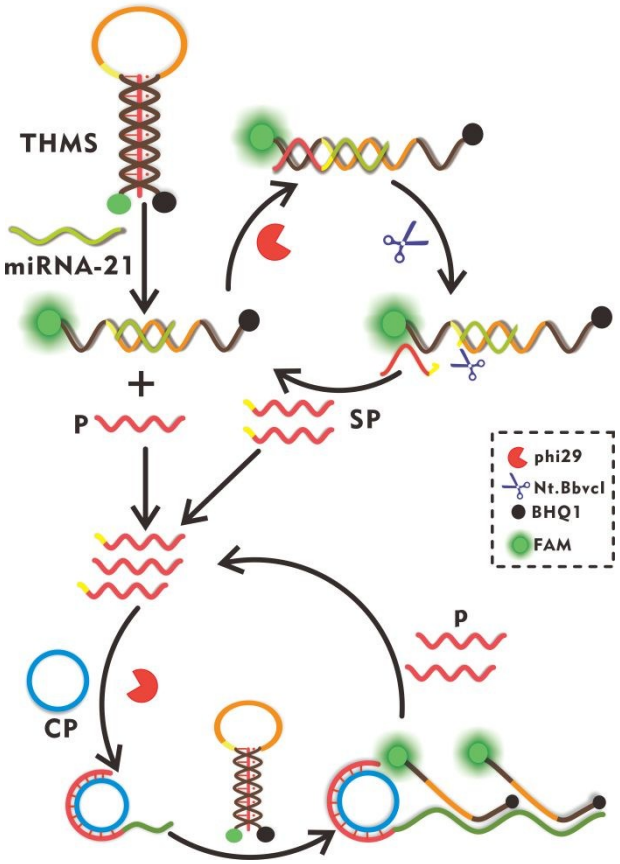

Scheme 1 Schematic illustration of fluorescence assay for miR-21 using THMS-actuated exponential RCA.

Scheme 1 illustrates the working principle of the proposed fluorescence biosensing strategy for ultrasensitive detection of miR-21. A THMS labeled with the fluorophore/quencher pair is ingeniously designed to contain typical triplex structure (T-A·T) in the stem region and long loop region that is comprised of a specific recognition sequence for nicking endonuclease (denoted in yellow), a complementary sequence for miR-21 (denoted in light green) and a RCA product (RT)-annealing sequence (denoted in dark green). In our assay, a circular probe (CP) is first prepared by using a padlock probe and a ligation probe via T4 DNA ligase-catalyzed ligation reaction. When target miR-21 is added into the system, miR-21 attaches with THMS, which induces the conformation change of THMS and the release of the trapped DNA (P, denoted in red) that can function as a primer for activating RCA reaction. With the aid of phi29 and dNTPs, miR-21 initiates an extension reaction, resulting in the formation of the recognition site for *Nt. BbvcI* in the generated DNA duplex. Immediately, *Nt. BbvcI* nicks the extended DNA segment, which releases a

single-stranded DNA that can act as the secondary RCA primer (SP, denoted in red). In the meanwhile, a new replicate site for phi29 is formed, initiating another round of "extension-nicking" reaction, thus a great many of RCA primers (Ps & SPs) is produced in the reaction solution. Subsequently, the primers anneal with the circular probes, triggering first-run RCA reaction in the presence of phi29 and dNTPs. As the resultant first-generation RT consists of numerous tandem repeated copies of circular template that can hybridize with the loop of THMS, the trapped DNA can be released, which act as primers for initiating new rounds of RCA reaction (second-run RCA). Followed by the cyclic RCA process, countless THMS is continuously consumed, thus significantly strong fluorescent signal can be achieved due to the separation between fluorophore (FAM) and quencher (BHQ1). In contrast, in the absence of target miR-21, THMS constructed by Watson-Crick and Hoogsteen interactions exists through stable triple-helix conformation in the solution, thus the fluorescence signal is negligible because of the fluorescence resonance energy transfer (FRET) phenomenon.[38, 39] Therefore, the proposed THMS-actuated exponential RCA strategy hold the potential for applying for miR-21 detection with high sensitivity.

3.2 Feasibility of THMS-actuated exponential RCA strategy for miR-21 detection

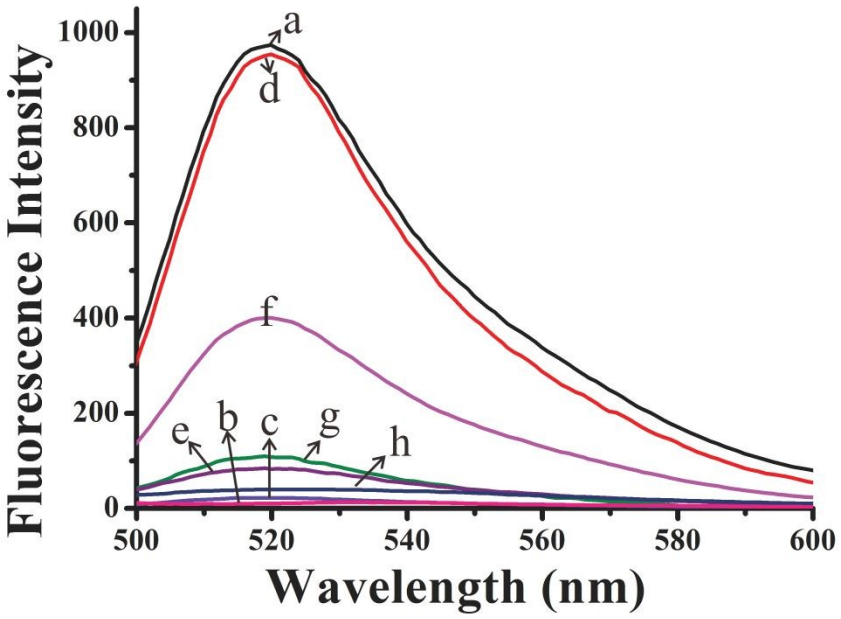

Fig. 1. Fluorescence emission spectra responses of the molecular switch

triplex-formation probe in reaction solution (a), the molecular switch triplex-formation probe incubated with the trapped DNA in reaction solution (b). Fluorescence emission spectra responses of this biosensor obtained upon analyzing the blank sample (c), the positive sample (d). The concentration of miR-21 is 100 nM. Curves e to h is for the feasibility research of the strategy which is controlled with no phi29 (e), no Nt.BbvCI (f), no circular template (g), miR-141 in place of miR-21 (h).

The stability of the triple helix in the reaction system was investigated by analyzing the fluorescence responses before and after the formation of the triplex state, and the results were shown in Fig. 1. After the incubation of the molecular switch triplex-formation probe in reaction solution, there was a very strong fluorescence signal due to the open conformation of triplex-formation probe (curve a). In contrast, when incubated the molecular switch triplex-formation probe with the trapped DNA in reaction solution, it was observed that a negligible fluorescence signal was obtained, which indicated the triplex formation induced the closure of the switch that resulted in the quenching of the fluorescence signal owing to the close proximity between FAM and BHQ1 in the triplex state (curve b). These data confirmed the high stability of the triple-helix structure in the reaction system. To verify the feasibility of our proposed strategy, different fluorescence responses obtained in a series of control experiments were depicted in Fig. 1. For the blank sample, an extremely weak fluorescence response was observed, signifying the fluorescence of fluorophore was completely extinguished by the quencher owing to FRET mechanism (curve c). In contrast, there was a significantly strong fluorescence signal with an emission peak at 520 nm for the positive sample (curve d). The signal-to-noise (S/N) of the strategy was reached to 42.3. These suggested target miR-21 induced the conformation switch of DNA triple helix that activated nicking endonuclease-assisted cyclic amplification and exponential RCA reaction. Additionally, when incubated THMS, CP, *Nt.BbvCI* with miR-21 in the absence of phi29, it was observed that a less strong fluorescence peak appeared in the curve, which demonstrated the fluorescence signal output was far away from enough only by target itself without enzymatic amplification (curve e). When incubated THMS, CP, phi29 with miR-21 in the absence of *Nt.BbvCI*, a

moderate fluorescence response was obtained with a S/N 17.69 (curve f). This implied nicking endonuclease-assisted cyclic amplification had a large share to the extremely high S/N. When incubated THMS, phi29, *Nt.BbvCI* with miR-21 in the absence of CP, we observed a relatively weak fluorescence signal similar with that of curve e, manifesting exponential RCA was crucial to achieve high sensitivity for miR-21 assay (curve g). Furthermore, when target miR-21 was replaced by non-target miR-141(curve h), there was a negligible fluorescence response, which confirmed the high specificity of this strategy for miR-21 detection. On the basis of the above results, it could clearly conclude the THMS-actuated exponential RCA strategy should be feasible for miR-21 detection.

3.3 Gel electrophoresis characterization

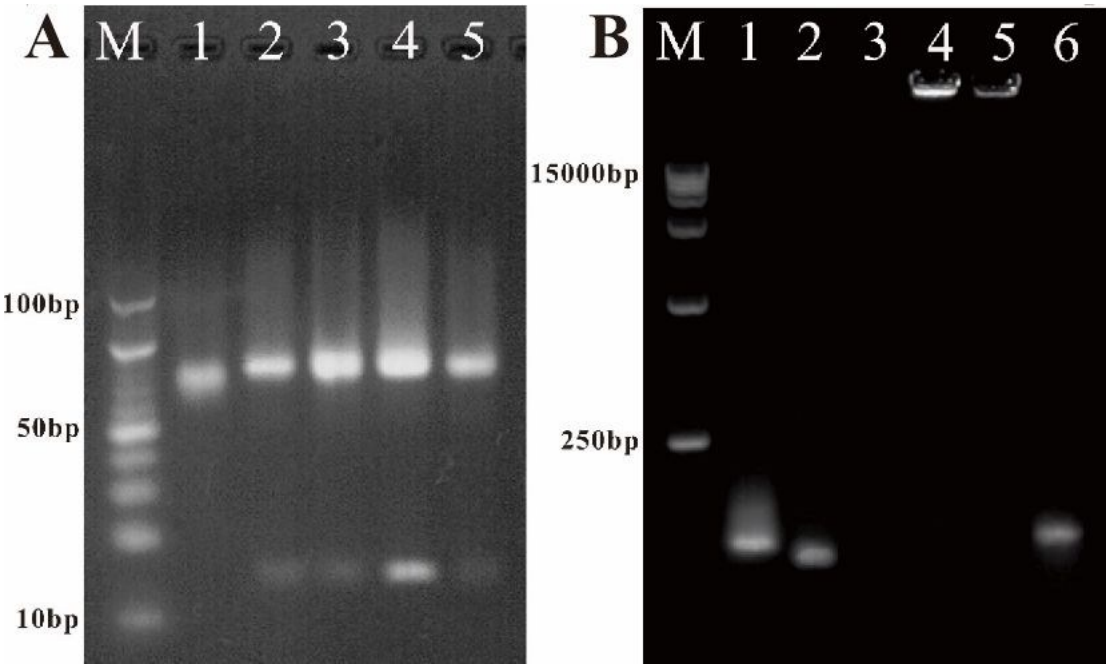

Fig. 2. (A) Gel electrophoresis image of THMS system and nicking endonuclease-assisted cyclic cleavage reaction. Lane M, DNA marker; Lane 1, THMS; Lane 2, THMS incubated with miR-21; Lane 3, THMS incubated with miR-21and phi29; Lane 4, THMS incubated with miR-21, phi29, and *Nt.BbvCI*; Lane 5, THMS incubated with miR-21 and *Nt.BbvCI*; (B) Gel electrophoresis image of THMS-actuated exponential RCA reaction. Lane M, DNA marker; Lane 1, padlock probe incubated with ligation probe and T4 DNA ligase; Lane 2, padlock probe incubated with ligation probe, T4 DNA ligase, Exo I, and Exo III; Lane 3, padlock

probe incubated with ligation probe, Exo I, and Exo III; Lane 4, RCA product; Lane 5, the positive sample; Lane 6, the blank sample.

To further verify the feasibility of the THMS-actuated exponential RCA reaction, gel electrophoresis analysis was performed, and the results were shown in Fig. 2. As seen in Fig. 2A, lane 1 displayed a bright band of our synthesized DNA triple-helix. When incubated THMS with miR-21, there were two bands at lane 2 on the image. The top band with slightly increased molecular weight represented the produced DNA duplex, and the bottom band signified the release of the trapped RCA primer. When incubated THMS, phi29 with miR-21, we observed the brightness of the top band was increased, while that of the bottom band was unchanged (lane 3). In contrast, when incubated THMS, phi29, and *Nt.BbvCI* with miR-21, it was found that the brightness of the bottom band characteristic for RCA primer was significantly increased, indicating the *Nt.BbvCI*-assisted circular strand displacement polymerization reaction induced the formation of numerous secondary RCA primers (lane 4). When incubated THMS, *Nt.BbvCI* with miR-21, there were two bands with the same mobility and intensity with that of lane 2 (lane 5). This suggested the circular strand displacement polymerization reaction and the formation of secondary RCA primers was activated by phi29. These data gave immediate evidence that one target molecule induced the formation of numerous RCA primer due to the *Nt.BbvCI*-assisted circular strand displacement polymerization reaction. Additionally, we further investigated THMS-actuated exponential RCA reaction by gel electrophoresis analysis. As seen in Fig. 2B, Lane M displayed the DNA marker (15000 bp). After the incubation of the padlock probe, ligation probe, and T4 DNA ligase, there was a bright band characteristic for the circular probe at lane 1. After the treatment with Exo I, and Exo III, a bright band with slightly decreased molecular weight was observed (lane 2). In contrast, after the incubation of the padlock probe, ligation probe, Exo I, and Exo III, it was found that no band appeared on the image (lane 3). It was reasonably concluded that the circular probe was successful prepared that could resist to enzymatic digestion. After the incubation of the circular probe, RCA primer, phi29, and dNTP, we observed a bright band with large-molecule-weight and particularly low mobility

appeared at lane 4, demonstrating the prosperous execution of RCA and the generation of RCA product. Furthermore, for the positive sample, a bright band characterized for large-molecular-weight of RCA product appeared on the image (lane 5). In contrast, for the blank sample, there was a band with similar mobility and brightness as that of lane 1 (lane 6). This indicated target-activated THMS induced the formation of numerous RCA primers that actuated exponential RCA reaction. These results gave immediate evidence that the proposed strategy could be used for amplified detection of miR-21.

3.4 Optimization of experimental conditions

To achieve the optimal analytical performances, several related experimental parameters including the reaction temperature, the reaction time, the amounts of phi29 and *Nt.BbvCI* were investigated, and the results were shown in Fig. 3. The reaction temperature would have an impact on not only the stability of DNA triple helix but also the activity of nucleic acid enzyme. The effect of the reaction time on the $(F_1-F_0)/F_0$ ratio was studied by probing the fluorescence intensities at 520 nm in the presence and absence of 1 nM miR-21. It was observed from Fig. 3A that the ratio increased with increasing of the reaction temperature at a lower temperature range, nevertheless, the ratio slowly decreased when the temperature was higher than 30 ℃. So, we chose 30 ℃ as the optimal temperature in the subsequent experiments. Additionally, we investigated the effect of the enzymatic reaction time on the fluorescence response (Fig. 3B). We observed the fluorescence intensities at 520 nm continuously increased with increasing of the reaction time and experienced almost no change for the positive sample when the reaction time was 4 h, whereas there was no obvious change for that of the blank sample. Thus, 4 h was selected as the optimal enzymatic reaction time. Furthermore, the amounts of phi29 and *Nt.BbvCI* can greatly influence the amplification efficiency of THMS-actuated exponential RCA. Fig. 3C and D depicted the fluorescence emission peak intensities of the biosensor in the presence and absence of 1 nM miR-21. As shown in Fig. 3C, for the positive sample, the fluorescence intensities at 520 nm gradually intensified with the increase of the concentration of phi29 and kept constant when the concentration was 2 U mL^{-1}. In

contrast, the fluorescence intensities changed little over the phi29 concentrations. Therefore, 2 U mL^{-1} was identified as the optimized concentration of phi29. Analogously, we selected 1 U mL^{-1} as the suitable concentration of *Nt.BbvCI* for the following experiments.

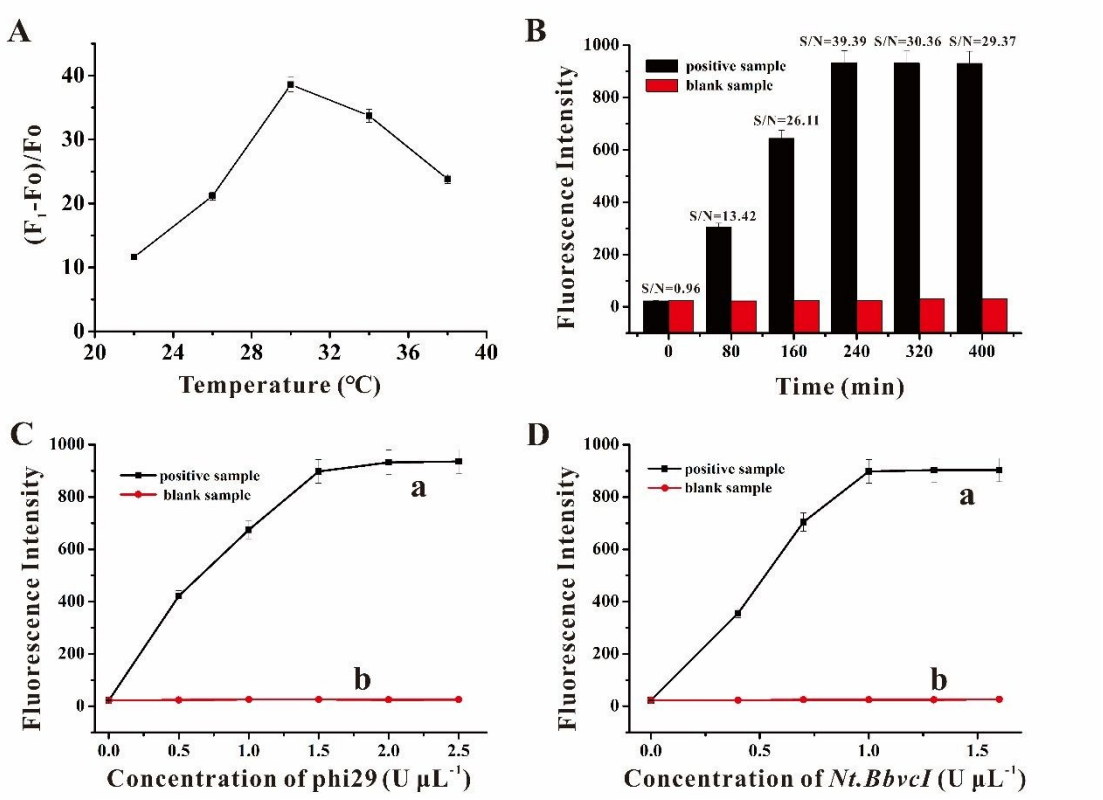

Fig. 3. (A) Effect of the reaction temperature on the $(F_1\text{-}F_0)/F_0$ value of the biosensor. F_1 and F_0 represent the fluorescence emission peak intensity at 520 nm in the presence and absence of 1 nM miR-21 respectively; (B) Effect of the enzymatic reaction time on the fluorescence response of the biosensor in the presence (the black bar) and absence (the red bar) of 1 nM miR-21; (C, D) Effect of the amount of phi29 (C) or *Nt.BbvCI* (D) on the fluorescence response of the biosensor in the presence (curve a) and absence (curve b) of 1 nM miR-21. Error bars are standard deviations across three repetitive experiments.

3.5 Analytical performance for miR-21 detection

Under the optimal experimental conditions, the analytical performance of the present strategy was investigated towards the detection of miR-21 at various concentrations. Fig. 4A showed the fluorescence emission spectra of the biosensor in

responses to different concentrations of miR-21. It was found that the fluorescence peak intensities accordingly increased with increasing of miR-21 concentrations, which indicates the fluorescence signal output was highly dependent on the concentration of miR-21. Fig. 4B depicted the linear correlation of the fluorescence intensities at 520 nm to the logarithm of the miR-21 concentrations ranging from 10 aM to 1 nM. The regression equation was F=355.4134+107.3559×logC with a correlation coefficient (R^2) of 0.9997, where F and C represented the fluorescence intensities at 520 nm and the miR-21 concentrations, respectively. The limit of detection (LOD) was calculated to be 1.1 aM by evaluating the average response of the blank sample plus 3 times standard deviation. In addition, the analytical performance of the proposed strategy for miR-21 assay was compared with those given by the existing methods, and the results were shown in Table 2. The data demonstrated the improved sensitivity and widened detection range was achieved owing to the efficient THMS-actuated exponential RCA strategy. Therefore, the constructed biosensor held great potential for miR-21 quantification with excellent sensitivity.

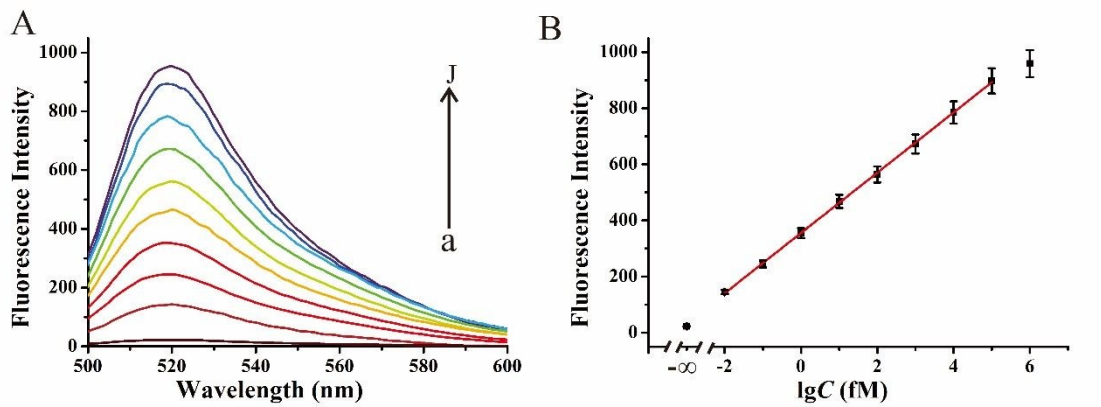

Fig. 4. (A) Fluorescence emission spectra responses to different concentrations of miR-21 (from curve a to l: 0, 10 aM, 100 aM, 1 fM, 10 fM, 100 fM, 1 pM, 10 pM, 100 pM, 1 nM); (B) The calibration curve of fluorescence intensities at 520 nm versus the logarithm of miR-21 concentrations. Error bars are standard deviations across three repetitive experiments.

3.6 Detection specificity

To evaluate the specificity of the proposed strategy, we challenged the system with target miR-21 and several non-target miRNAs including miR-141, let-7a, miR-144, and miR-155. As seen in Fig. 5, a remarkably strong fluorescence signal was obtained in the presence of miR-21. In contrast, there was negligible fluorescence signal for the negative control without miR-21 or any of these competing non-target miRNAs. These results confirmed the high specificity of this strategy for miR-21 detection.

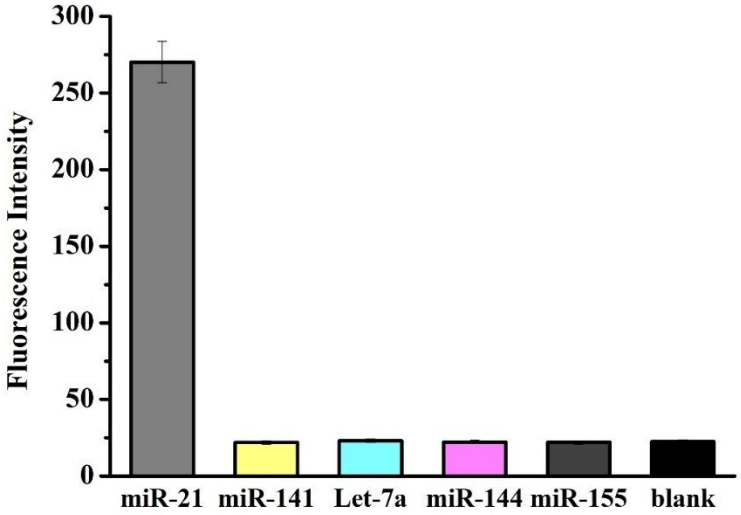

Fig. 5. Plot of fluorescence intensity at 520 nm obtained with different miRNAs. The concentration of miR-21 is 100 aM. The concentration of non-target miRNAs is 10 fM. Error bars are standard deviations across three repetitive experiments.

3.7 Real sample analysis

To further demonstrate whether the feasibility of this strategy in a real sample that was extracted from breast cancer cell (MCF-7) and a pancreatic cancer cell line (AsPc-1) as an example. According to previous reports,[40] miR-21 is closely related to the proliferation and expression of MCF-7 cells. Meanwhile, it has been reported that miR-21 overexpression is closely related to pancreatic cancer. Some studies have selected AsPc-1 cells to miR-21 studied,[41, 42] so we used MCF-7 cells and AsPc-1 cells as examples. As shown in Fig. 6, by using RT-PCR technology to detect two groups of samples, the results showed that the expression of miR-21 was significantly

different in the two cancer cells lysates, and the miR-21 in the cell lysate of MCF-7 was higher than AsPc-1. The amount of miR-21 measured by this method was converted to the number of copies of the miRNA molecule to permit comparisons. the results obtained by our proposed strategy were consistent with those by RT-PCR, indicating the accuracy and reproducibility of the method and its potential in clinical samples.

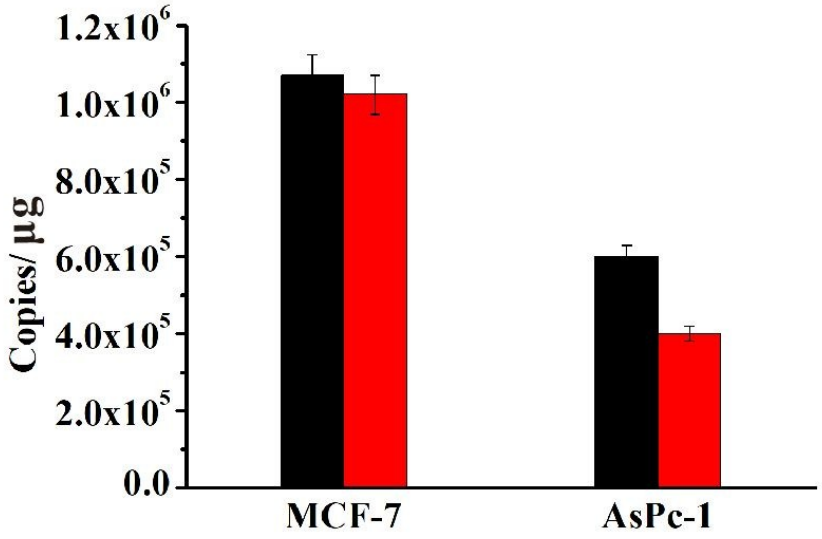

Fig. 6. Real sample application of miR-21 detection in cell lysates of MCF-7 and AsPc-1 cells. Pillars represent the amount of copies of miR-21 per microgram determined using the proposed strategy (black pillars) and RT-PCR method (red pillars).

4. Conclusion

In summary, a rapid and highly efficient fluorescence biosensor for the ultrasensitive detection of miR-21 was successfully constructed using target-induced the THMS conformation change-initiated exponential RCA reaction. In this work, target attaches with the THMS resulting in the conformation change of that and a concurrent "extension-nicking" process, which induces the generation of multiple primer (Ps & SPs) for triggering the exponential RCA reaction. Intriguingly, the use of a skillfully designed THMS not only contains a primer for RCA but also functions as the tracer for fluorescence assay. Moreover, this biosensor is demonstrated to enable accurate detection of miR-21 with improved detection limit as low as 1.1 aM

owing to the high efficiency and rapid amplification kinetics of exponential RCA, and analyze complicated biological samples. Therefore, the facile and robust exponential RCA strategy based on multiple generation modes of primer indeed establishes a biosensing platform for detecting low levels of analytes in clinical diagnosis and fundamental biomedicine research.

Acknowledgements

This work was supported by National Natural Science Foundation of China (31471644), the Primary Research & Development Plan of Shandong Province (2017GSF220009), the Program for Taishan Scholar of Shandong Province (ts201712048).

References

1. Y. Cheng, X. Zhang, Z. Li, X. Jiao, Y. Wang and Y. Zhang, Angew. Chem., 2009, 48, 3268-3272. 2009, 48, 3268-3272.
2. Z. Wang, J. Zhang, F. Chen and K. Cai, Analyst., 2017, 142, 2796-2804.
3. F. Yang, Y. Cheng, Y. Cao, H. Dong, H. Lu, K. Zhang, X. Meng, C. Liu and X. Zhang, Chem. Sci., 2019, 10, 1709-1715.
4. K. Guk, S. G. Hwang, J. Lim, H.-Y. Son, Y. Choi, Y.-M. Huh, T. Kang, J. Jung and E.-K. Lim, Chem. Commun., 2019, 55, 3457-3460.
5. H. Yan, U. Bhattarai, Z.-F. Guo and F.-S. Liang, J. Am. Chem. Soc., 2017, 139, 4987-4990.
6. Q. Li, F. Zeng, N. Lyu and J. Liang, Analyst., 2018, 143, 2304-2309.
7. D. Yang, W. Cheng, X. Chen, Y. Tang and P. Miao, Analyst., 2018, 143, 5352-5357.
8. J. Wang, T. Li, R. Shen and G. Li, Anal. Chem., 2019, 91, 3429-3435.
9. S. Chirayil, R. Chirayil and K. J. Luebke, Nucleic acids research, 2009, 37, 5486-5497.
10. E. Varallyay, J. Burgyan and Z. Havelda, Nature protocols, 2008, 3, 190-196.
11. P. Gai, C. Gu, H. Li, X. Sun and F. Li, Anal. Chem., 2017, 89, 12293-12298.
12. T. Hou, N. Xu, W. Wang, L. Ge and F. Li, Anal. Chem., 2018, 90, 9591-9597.
13. R. M. Torrente-Rodriguez, S. Campuzano, V. Ruiz-Valdepenas Montiel, J. J. Montoya and J. M. Pingarron, Biosens. Bioelectron., 2016, 86, 516-521.
14. B. Yao, S. Zhu, X. Xu, N. Feng, Y. Tian and N. Zhou, Analyst., 2019, 144, 2179-2185.
15. X. Fan, Y. Qi, Z. Shi, Y. Lv and Y. Guo, Sens. Actuators, B., 2018, 255, 1582-1586.
16. C. Shi, Q. Liu, C. Ma and W. Zhong, Anal. Chem., 2014, 86, 336-339.
17. Q. Li, Z. Liu, D. Zhou, J. Pan, C. Liu and J. Chen, Analyst, 2019, 144, 2173-2178.
18. S. Ou, T. Xu, X. Liu, X. Yu, R. Li, J. Deng, J. Yuan and Y. Chen, Sens.

View Article Online
DOI: 10.1039/C9AN00953A

Actuators, B., 2018, 255, 3057-3063.
19. R. Deng, L. Tang, Q. Tian, Y. Wang, L. Lin and J. Li, Angew. Chem., 2014, 53, 2389-2393.
20. S. Wang, S. Lu, J. Zhao, J. Ye, J. Huang and X. Yang, Biosens. Bioelectron., 2019, 126, 565-571.
21. Q. Tian, Y. Wang, R. Deng, L. Lin, Y. Liu and J. Li, Nanoscale, 2015, 7, 987-993.
22. X. Xu, H. Wei and W. Jiang, Analyst., 2017, 142, 2247-2252.
23. L. Huang, D.-B. Wang, N. Singh, F. Yang, N. Gu and X.-E. Zhang, Nanoscale, 2018, 10, 20289-20295.
24. B. Liu, B. Zhang, G. Chen, H. Yang and D. Tang, Anal. Chem., 2014, 86, 7773-7781.
25. L. Tang, Y. Liu, M. M. Ali, D. K. Kang, W. Zhao and J. Li, Anal. Chem., 2012, 84, 4711-4717.
26. W. Yu, J. Li, C. Zuo, Y. Tao, S. Bai, J. Li, Z. Zhang and G. Xie, Anal. Chim. Acta., 2019, 1068, 96-103.
27. T. N. Grossmann, L. Roglin and O. Seitz, Angew. Chem., 2007, 46, 5223-5225.
28. F. Iacovelli, A. Idili, A. Benincasa, D. Mariottini, A. Ottaviani, M. Falconi, F. Ricci and A. Desideri, J. Am. Chem. Soc., 2017, 139, 5321-5329.
29. X. Wu, B. Guo, Y. Sheng, Y. Zhang, J. Wang, S. Peng, L. Liu and H.-C. Wu, Chem. Commun., 2018, 54, 7673-7676.
30. A. Idili, A. Vallee-Belisle and F. Ricci, J. Am. Chem. Soc., 2014, 136, 5836-5839.
31. E. Xiong, Z. Li, X. Zhang, J. Zhou, X. Yan, Y. Liu and J. Chen, Anal. Chem., 2017, 89, 8830-8835.
32. W. Yang, Y. Shen, D. Zhang and W. Xu, Chem. Commun., 2018, 54, 10195-10198.
33. P. Tang, J. Zheng, J. Tang, D. Ma, W. Xu, J. Li, Z. Cao and R. Yang, Chem. Commun., 2017, 53, 2507-2510.
34. S. Ranallo, C. Prevost-Tremblay, A. Idili, A. Vallee-Belisle and F. Ricci, Nat. Commun., 2017, 8, 1-9.
35. J. Zheng, J. Li, Y. Jiang, J. Jin, K. Wang, R. Yang and W. Tan, Anal. Chem., 2011, 83, 6586-6592.
36. B. Guo, Y. Sheng, K. Zhou, Q. Liu, L. Liu and H.-C. Wu, Angew. Chem., 2018, 57, 3602-3606.
37. S. Lu, S. Wang, J. Zhao, J. Sun and X. Yang, ACS Sens., 2018, 3, 2438-2445.
38. F. D. Lewis, L. Zhang and X. Zuo, J. Am. Chem. Soc., 2005, 127, 10002-10003.
39. J. N. Miller, Analyst., 2005, 130, 265-270.
40. A. M. Krichevsky and G. Gabriely, J Cell Mol Med., 2009, 13, 39-53.
41. M. Bloomston, W. L. Frankel, F. Petrocca, S. Volinia, H. Alder, J. P. Hagan, C. G. Liu, D. Bhatt, C. Taccioli and C. M. Croce, Jama., 2007, 297, 1901-1908.

42. T. A. Mace, A. L. Collins, S. E. Wojcik, C. M. Croce, G. B. Lesinski and M. Bloomston, J Surg Res., 2013, 184, 855-860.